



HAL
open science

Fused Particle Fabrication 3-D Printing: Recycled Materials' Optimization and Mechanical Properties

Aubrey L. Woern, Dennis J. Byard, Robert B. Oakley, Matthew J. Fiedler,
Samantha L. Snabes, Joshua M. Pearce

► **To cite this version:**

Aubrey L. Woern, Dennis J. Byard, Robert B. Oakley, Matthew J. Fiedler, Samantha L. Snabes, et al.. Fused Particle Fabrication 3-D Printing: Recycled Materials' Optimization and Mechanical Properties. *Materials*, 2018, 11 (8), pp.1413. 10.3390/ma11081413 . hal-02111365

HAL Id: hal-02111365

<https://hal.science/hal-02111365>


Submitted on 26 Apr 2019

HAL is a multi-disciplinary open access archive for the deposit and dissemination of scientific research documents, whether they are published or not. The documents may come from teaching and research institutions in France or abroad, or from public or private research centers.

L'archive ouverte pluridisciplinaire **HAL**, est destinée au dépôt et à la diffusion de documents scientifiques de niveau recherche, publiés ou non, émanant des établissements d'enseignement et de recherche français ou étrangers, des laboratoires publics ou privés.

Article

Fused Particle Fabrication 3-D Printing: Recycled Materials' Optimization and Mechanical Properties

Aubrey L. Woern ¹, Dennis J. Byard ¹, Robert B. Oakley ², Matthew J. Fiedler ^{2,3},
Samantha L. Snabes ^{2,3} and Joshua M. Pearce ^{3,4,5,*} 

¹ Department of Mechanical Engineering–Engineering Mechanics, Michigan Technological University, Houghton, MI 49931, USA; alwoern@mtu.edu (A.L.W.); djbyard@mtu.edu (D.J.B.)

² re:3D Inc., 1100 Hercules STE 220, Houston, TX 77058, USA; robert.oakley@re3d.org (R.B.O.); matthew@re3d.org (M.J.F.); samantha@re3d.org (S.L.S.)

³ Department of Material Science and Engineering, Michigan Technological University, Houghton, MI 49931, USA

⁴ Department of Electrical and Computer Engineering, Michigan Technological University, Houghton, MI 49931, USA

⁵ Department of Electronics and Nanoengineering, School of Electrical Engineering, Aalto University, 00076 Espoo, Finland

* Correspondence: pearce@mtu.edu or joshua.pearce@aalto.fi; Tel.: +01-906-487-1466

Received: 21 July 2018; Accepted: 9 August 2018; Published: 12 August 2018



Abstract: Fused particle fabrication (FPF) (or fused granular fabrication (FGF)) has potential for increasing recycled polymers in 3-D printing. Here, the open source Gigabot X is used to develop a new method to optimize FPF/FGF for recycled materials. Virgin polylactic acid (PLA) pellets and prints were analyzed and were then compared to four recycled polymers including the two most popular printing materials (PLA and acrylonitrile butadiene styrene (ABS)) as well as the two most common waste plastics (polyethylene terephthalate (PET) and polypropylene (PP)). The size characteristics of the various materials were quantified using digital image processing. Then, power and nozzle velocity matrices were used to optimize the print speed, and a print test was used to maximize the output for a two-temperature stage extruder for a given polymer feedstock. ASTM type 4 tensile tests were used to determine the mechanical properties of each plastic when they were printed with a particle drive extruder system and were compared with filament printing. The results showed that the Gigabot X can print materials $6.5\times$ to $13\times$ faster than conventional printers depending on the material, with no significant reduction in the mechanical properties. It was concluded that the Gigabot X and similar FPF/FGF printers can utilize a wide range of recycled polymer materials with minimal post processing.

Keywords: 3-D printing; additive manufacturing; distributed manufacturing; open-source; polymers; recycling; waste plastic; extruder; upcycle; circular economy

1. Introduction

With the introduction of the self-replicating rapid prototyper (RepRap) 3-D printer [1–3], the costs of additive manufacturing (AM) with 3-D printers have been reduced enough to be accessible to consumers. This has allowed for the emergence of a distributed manufacturing paradigm in AM [4–6], where 3-D printing can be used to manufacture products for the consumer and by the consumer directly, with significant savings compared to the purchasing of mass-manufactured products [7–12]. The emerging support for this model in the business literature [13–15] is in part due to the exponential rise of free digital design file sharing for 3-D printed products [12], which ranges from sophisticated scientific instruments [16–20] to everyday toys for children and cosplayers [10]. Regardless of the

sophistication of the product, high return on investments (ROIs) can be enjoyed based on the download substitution values using commercial polymer 3-D printing filament [21,22]. Commercial filament, however, is marked up significantly (e.g., $>5\times-10\times$) over the cost of the raw polymers, which limits the cost savings and thus, the deployment velocity of distributed manufacturing to further increase the rate of accessibility of AM [23]. The negative effects of the high costs of filament are most notable for large format 3-D printers (those with a build volume that is greater than a cubic foot), which can process several kg of polymer in a single print lasting over 24 h.

One method of overcoming these cost barriers is to use a means of distributed plastic recycling, involving upcycling plastic waste into 3-D printing filament with a recyclebot (an open source waste plastic extruder [24]). Previous research on the life cycle analysis of the recyclebot process found a 90% decrease in the embodied energy of the filament from the acquiring, processing of the natural resources, and the synthesizing compared to traditional filament manufacturing [25–27]. This allows for the tightening of the loop of the circular economy [28] because it enables real distributed recycling that eliminates nearly all energy use and pollution from transportation. Many recyclebot versions have been developed including open source variations from the Plastic Bank, Filastruder, Precious Plastic, Lyman, and Perpetual Plastic, as well as fully commercial versions including the Filastruder, Filafab, Noztek, Filabot, EWE, Extrusionbot, Filamaker (also has a shredder), and the Strooder, Felfil (OS) [29]. Most recently, a “RepRapable Recyclebot” has been demonstrated [30], where most of the machine’s parts can be 3-D printed from waste plastic themselves. Several polymers have been successfully recycled as single component thermoplastic filaments, such as polylactic acid (PLA) [30–34], high-density polyethylene (HDPE) [24,35,36], acrylonitrile butadiene styrene (ABS) [28,36,37], elastomers [9], as well as composites (e.g. waste wood [38] and carbon fiber reinforced [39]).

Unfortunately, each time a polymer is heated and extruded (whether it be in the recyclebot filament making process or during conventional fused filament fabrication (FFF)/fused deposition modeling (FDM) 3-D printing), the mechanical properties are degraded [31,32,40,41]. This effectively limits this process of recycling to 5 cycles [31,32] without the use of blending virgin materials or adding materials for mechanical property reinforcement. To reduce the number of melt/extrude cycles of recycled plastic that is used for 3-D printing, one option is to eliminate the need for filament and print directly from pellets, flakes, regrind, or shreds of recycled plastic, which will be referred to as particles here. Several 3-D printers using fused particle fabrication (FPF) (or fused granular fabrication (FGF)) have been designed to accomplish this in the academic [42–44], hobbyist [43–45], and commercial systems [46–50]. These systems have been tested with virgin pellets, however the mechanical properties of FPF printers using recycled polymer particles of various shapes and sizes has not been reported, which limits the ability of engineers to fabricate load bearing products from recycled waste using FPF 3-D printing.

In this study, the open source Gigabot X [51], which is a large scale recycled plastic 3-D printer, was used to fabricate and test the mechanical properties of parts that were made using FPF to fill this knowledge gap. To establish a baseline, virgin PLA pellets were analyzed first and were then compared to four recycled polymers: (1) PLA regrind of 3-D printed parts (the most common 3-D printed plastic), (2) recycled ABS pellets (the second most common 3-D printed plastic), (3) recycled polyethylene terephthalate pellets (PET, the most common waste plastic [52]), and (4) recycled polypropylene chips (PP, the second most common waste plastic [52]). First, the material size characteristics were quantified using digital image processing. Then, a power and nozzle velocity matrix printing test were completed to determine the optimum print speed and temperature settings for a given polymer feedstock. During this phase of testing, any problems with bed adhesion and warping were identified and resolved. Third, a set of ASTM type 4 tensile bars were printed and were pulled to confirm the mechanical properties of the plastic when it was printed with a pellet drive extruder system and was compared with the results of past work with FFF/FDM 3-D printers, while noting the number of melt cycles.

2. Materials and Methods

2.1. Materials

Virgin 4043D PLA pellets were obtained from Nature Works LLC. PLA regrind was obtained from a mixture of failed 3-D prints from various sources of filaments and was ground with an open source grinder [53]. PP regrind was provided by McDonnough Plastics. Northwest Polymers and CiorC provided ABS and PET recycled materials. The size characteristics of the particles for each starting material were quantified using digital imaging and the open source Fiji/ImageJ [54].

2.2. FPF 3-D Printer

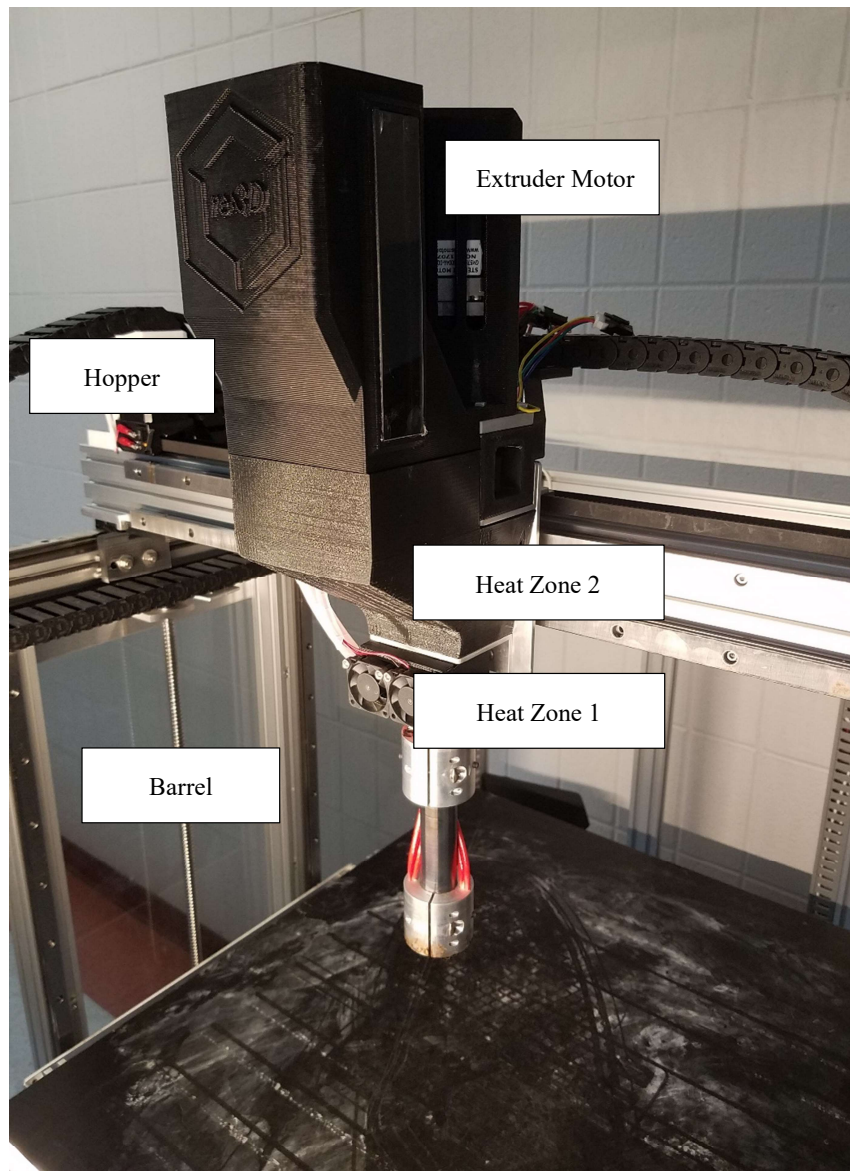
A prototype Gigabot X [55] was used to print the materials. The prototype used an extruder system that was closely related to an industrial thermoplastic extruder, however it was scaled down and mounted as the extruder head of the 3-D printer. The extrusion screw was designed with an increasing diameter down the length of the screw with a ratio of 2.5:1 from the start to the end [55]. The motor driving the extrusion screw was a NEMA 23 stepper motor with a planetary gearbox with an 18:1 reduction. This ran off an external stepper driver [55]. The hopper was 3-D printed to allow for ease of modification and optimization of the design during testing. The extruder was heated by four 60-watt 24-volt heater cartridges that were placed in groups of two in strategic locations on the barrel [55]. Figure 1a shows a Gigabot X (the parts are labeled along with the heating zones) and Figure 1b shows the details of the extruder in a cutaway computer aided design (CAD) model with the major components labeled. Full details of the design can be found at reference [55]. 3-D models were sliced with Slic3r [56] and the printer was controlled with Marlin Firmware [57]. The testing procedures were then developed for an FPF platform to allow for the data to be collected efficiently for each plastic. These data can be collected in a couple of working days and provide information on the optimum settings regardless of what type of plastic is used. This is beneficial for expediting the continued work on this or similar platforms with new polymers, additives, and composites.

2.3. Optimization of Temperature and Speed

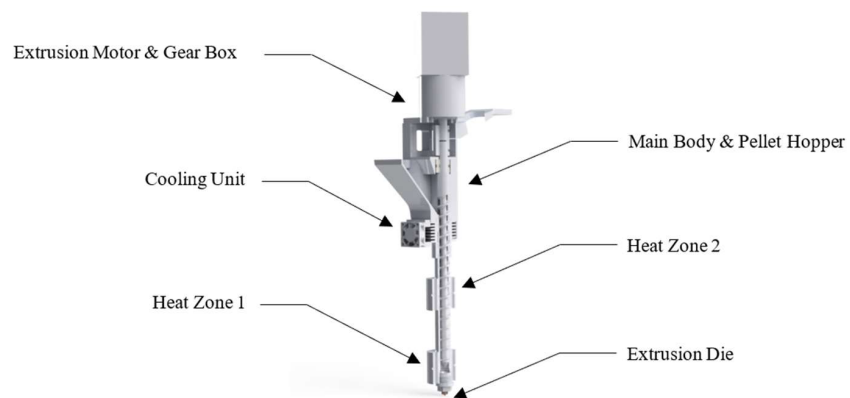
The power vs. velocity matrix testing was accomplished by first identifying the upper and lower bounds of the printable temperature range of a given plastic through literature research, as summarized in Table 1.

Table 1. 3-D printable temperature range for the two most common 3-D printed polymers and the two most common post-consumer waste polymers.

Material	Temperature Range °C	Source
PLA	160–200	[58]
ABS	200–250	[59]
PET	200–240	[60]
PP	170–250	[61]



(a)



(b)

Figure 1. (a) The open source Gigabot X with the major components labeled. (b) Details of the extruder.

Heating zones 1 (tip of the nozzle) and 2 inside the barrel were then set to every combination of temperatures in the printable temperature range at an appropriate resolution to capture the entire spectrum. A series of double lines were then printed at each temperature combination at print speeds from 5 to 50 mm/s in 5 mm/s increments [62]. The printed lines (example in Figure 2) were then massed on a digital scale (± 0.01 g) and the line masses were compared to the theoretical line mass. The objective of this test was to find both the optimum print speed and the temperature settings for the extruder for each 3-D printing material. The optimum settings were determined both by the temperature settings that had the lowest standard deviation in terms of the line weight for a set of lines and the print speeds across all of the temperature settings, which resulted in the heaviest line masses.



Figure 2. Materials Sample Matrix Test (polylactic acid (PLA) shown).

A single walled vase test [63] was used to determine the ideal settings for the flow percentage and the actual extrusion width once the print speed and the temperature zone settings had been confirmed. To conduct this test, a single walled hollow cylinder with known theoretical dimensions was printed. Once the print was completed, the specimen's mass was recorded and was compared to the theoretical mass of the component using the specific density of the plastic that was used. The method of similar triangles was then used to determine the appropriate flow percentage. Once the flow percentage was successfully calibrated, digital calipers (± 0.005) were used to find the printed wall thickness. This value was then loaded into the slicing software (Slic3r) so that the printed line width could be corrected for in the slicing software.

2.4. Tensile Testing

Tensile testing was first completed on PLA using the ASTM D638 Type 1 and Type 4 standard tensile bars. For PLA, Types 1 and 4 were used to examine any potential difference in mechanical performance due to the smaller geometry of the Type 4 tensile test bars, as has been done before with more conventional FFF based 3-D printing [64]. This was a point of concern due to the relatively large size of the printer nozzle diameter (1.75 mm) compared to the smallest dimension of the Type 4 tensile bars (2 mm). The remainder of the tensile testing was completed using ASTM D638 Type 4 standard tensile bars. The bars were printed at ideal print settings that were found during matrix testing at 100% infill. The infill pattern was set to 0 degrees or "perpendicular" with respect to the long axis of the tensile bars. The samples were then pulled until failure using a 5000 lb. load cell (Model LCF455). The strain data was captured using a 1-inch Epsilon extensometer (Model E95691, Error: ± 0.0276 mm).

3. Results

3.1. Materials Size Distribution

Digital images of the input polymer materials are shown in Figures 3–7 for virgin PLA, recycled PLA, ABS, PET, and PP, respectively. In each Figure, the inset shows the particle size distribution for the material. The virgin PLA had the most uniform particles as well as the most spherical shape which provided the best feeding. The recycled polymers, however, had much larger size distributions. The regrind polypropylene and regrind PLA were the least consistent. Both of the reground plastics consisted of flakes, dust-like particles, and large chunks, all of which surprisingly fed nicely into the auger system without jamming or miss-feeding. It was concluded that pellets with areas smaller than 22 mm² could feed into the auger regardless of shape.

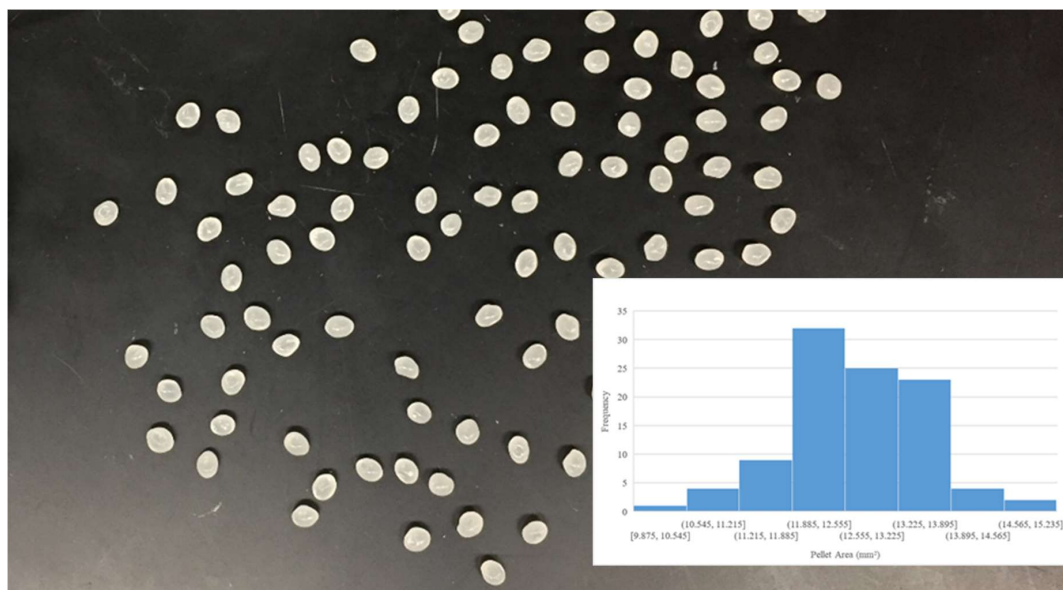


Figure 3. Virgin PLA pellet size distribution.

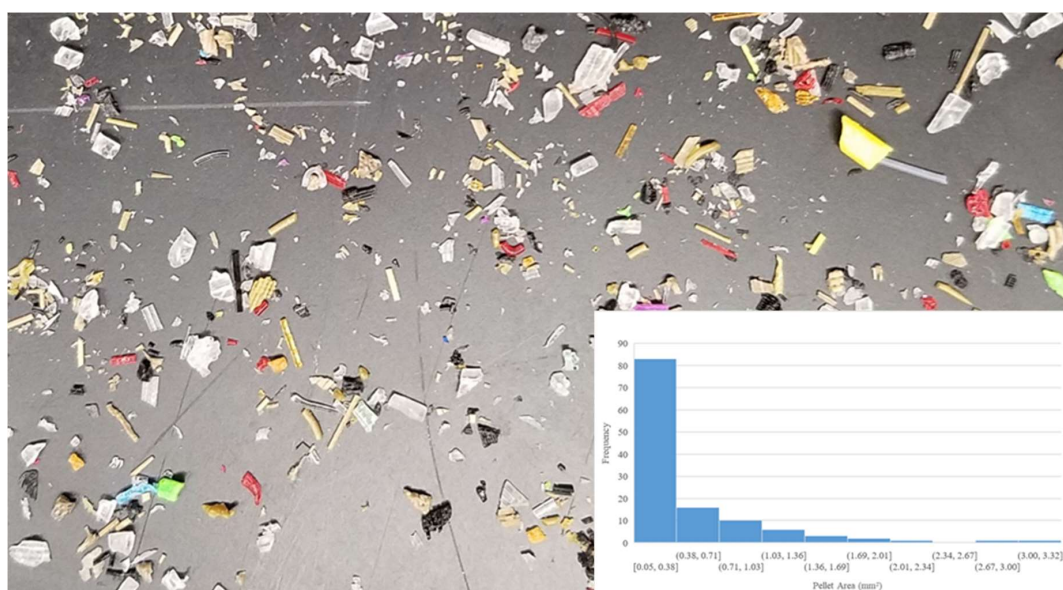


Figure 4. Reground 3-D printed PLA size distribution.

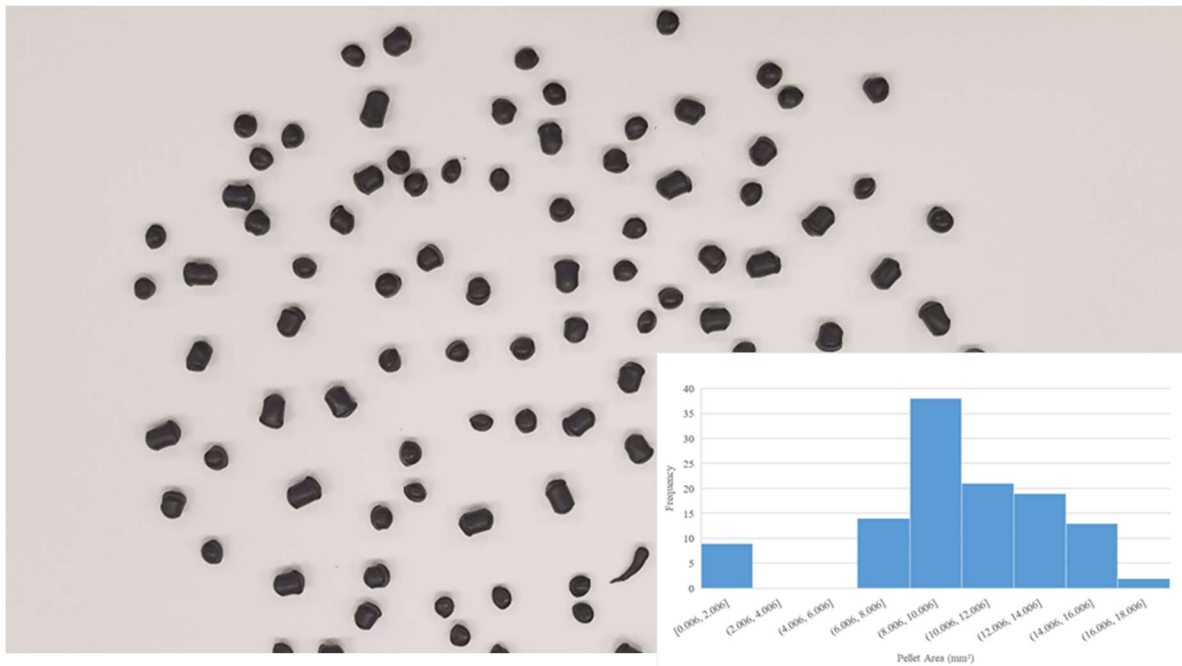


Figure 5. Recycled acrylonitrile butadiene styrene (ABS) pellet size distribution.

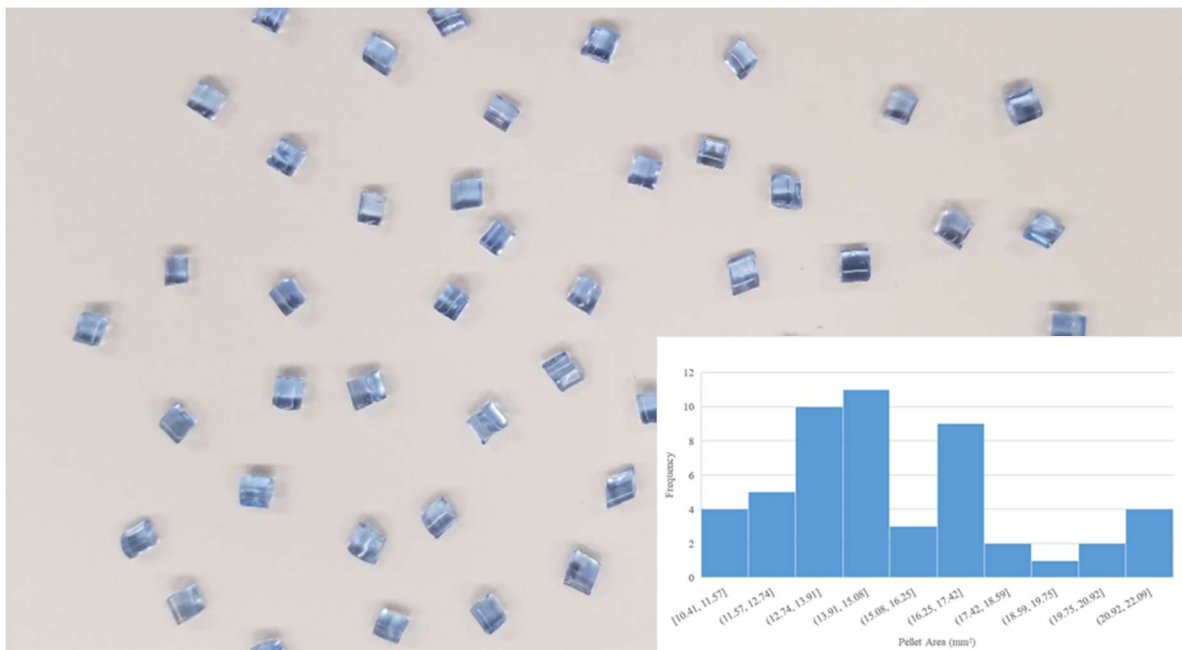


Figure 6. Recycled as well as the two most common waste plastics (polyethylene terephthalate (PET) size distribution.



Figure 7. Recycled polypropylene (PP) flake size distribution.

3.2. Optimal Printing Temperatures and Velocities

For each polymer, a matrix was generated for the range of the operating temperatures for the two temperature zones as well as the nozzle velocities from 5 to 50 mm/s. The difference between the theoretical and the actual mass of the line is shown as a function of the nozzle speeds. The color coding on the charts represent how different each actual line mass is compared to its ideal mass. The farther away from the ideal, the redder the number becomes. For the main part of the chart, zero would be ideal, and the farther away from zero, the worse the sample was and the redder it is. For the average and standard deviation section, the more green the number is, the closer the average was to its ideal mass. The standard deviation tells us how much each mass varied with one another. The ideal temperature combination is one that has a low average difference and a low standard deviation.

3.2.1. Virgin PLA

Figure 8 shows the results for virgin PLA. The ideal temperature settings were found to be 160 and 200 °C for heat zones 1 and 2, respectively. In examining the general trend across the matrix, also note that higher zone 1 temperatures, with respect to zone 2, results in a higher standard deviation for a given line test. This has been corroborated by initial literature research [65]. This phenomenon is attributed to the specific density differential of the plastic across zones 1 and 2, creating a stabilizing back pressure at the extrusion die.

Speed (mm/s)	Temperature (°C)																								
	Zone 2: 160 170 180 190 200					160 170 180 190 200					160 170 180 190 200					160 170 180 190 200									
	Zone 1: 160 160 160 160 160					170 170 170 170 170					180 180 180 180 180					190 190 190 190 190					200 200 200 200 200				
5	1.17	0.97	0.67	0.27	0.27	0.67	-0.03	-0.13	0.67	-0.03	1.57	0.97	1.07	0.17	-0.33	1.37	0.37	-0.03	-0.83	-0.03	-0.83	-0.03	-0.23	-0.03	0.27
10	0.67	-0.03	-0.13	0.17	0.27	0.47	-0.23	-0.23	0.67	-0.13	0.67	-0.03	-0.63	-0.93	-0.53	0.57	-0.43	-0.73	-0.83	-0.73	-0.93	-0.63	-0.03	-0.63	-0.93
15	0.37	-0.03	-0.13	-0.03	0.17	0.47	-0.23	-0.23	0.47	-0.23	0.07	-0.43	-0.73	-0.83	-0.53	0.07	-0.43	-0.73	-0.73	-0.73	-0.73	-0.73	-0.13	-0.73	-1.03
20	0.57	-0.03	-0.23	-0.13	-0.03	1.07	-0.13	-0.23	-0.33	-0.13	0.47	-0.03	-0.33	-0.63	-0.63	0.57	-0.03	-0.63	-0.73	-0.63	-0.73	-0.43	0.37	-0.43	-0.83
25	0.97	0.07	-0.23	-0.13	0.07	1.07	-0.03	-0.23	-0.33	-0.23	0.77	-0.03	-0.33	-0.43	-0.33	0.97	0.07	-0.43	-0.53	-0.43	-0.63	-0.33	0.47	-0.33	-0.63
30	0.97	0.07	-0.03	-0.03	0.07	1.17	-0.03	-0.33	-0.43	-0.03	1.17	0.17	-0.13	-0.33	-0.33	1.07	0.07	-0.23	-0.43	-0.23	-0.63	-0.03	0.77	-0.03	-0.43
35	0.97	0.17	-0.23	0.17	0.07	1.37	0.47	-0.03	-0.23	-0.13	1.07	0.67	0.07	-0.13	-0.33	1.07	0.67	-0.23	-0.33	-0.23	-0.43	-0.03	0.77	-0.03	-0.33
40	1.37	0.57	-0.13	-0.13	0.07	1.17	0.67	-0.13	-0.13	0.07	1.07	1.07	-0.03	-0.23	-0.33	1.27	0.77	-0.03	-0.33	-0.03	-0.53	0.27	0.67	0.27	-0.23
45	1.27	0.57	-0.13	-0.13	-0.03	1.27	0.57	-0.13	-0.13	-0.13	1.37	0.87	0.07	-0.43	-0.23	1.17	0.87	0.17	-0.33	0.17	-0.43	0.37	0.77	0.37	-0.03
50	1.37	0.87	-0.13	-0.43	-0.13	1.17	0.67	-0.13	-0.13	-0.33	1.17	1.27	0.47	-0.43	-0.43	1.27	0.97	0.27	-0.23	0.27	-0.53	0.47	0.77	0.47	0.47
Average	0.97	0.32	-0.07	-0.04	0.08	0.99	0.17	-0.18	0.01	-0.13	0.94	0.45	-0.05	-0.42	-0.40	0.94	0.29	-0.26	-0.53	-0.26	-0.64	-0.11	0.42	-0.11	-0.37
Abs. Value of Avg.	0.97	0.32	0.07	0.04	0.08	0.99	0.17	0.18	0.01	0.13	0.94	0.45	0.05	0.42	0.40	0.94	0.29	0.26	0.53	0.26	0.64	0.11	0.42	0.11	0.37
Standard Deviation	0.33	0.37	0.25	0.19	0.12	0.31	0.36	0.08	0.40	0.11	0.42	0.56	0.50	0.31	0.12	0.39	0.49	0.34	0.22	0.34	0.16	0.39	0.39	0.39	0.48

Best Temperature Settings

Figure 8. PLA Virgin-Difference between the theoretical and actual mass of the line-speed temperature matrix.

Observing the trend in the average line weight speeds across the full temperature spectrum, line weight is maximized at print speeds of around 20 mm/s, as shown in Figure 9. At this print speed, the volumetric deposition rate of the printer is 35 mm³/s. In comparison, a traditional FFF printer at a print speed of 50 mm/s, with print settings of 0.2 mm layer height with a 0.4 mm nozzle, will average at 4 mm³/s. This translates to an 8.75x increase in the speed of the 3-D printed part formation.

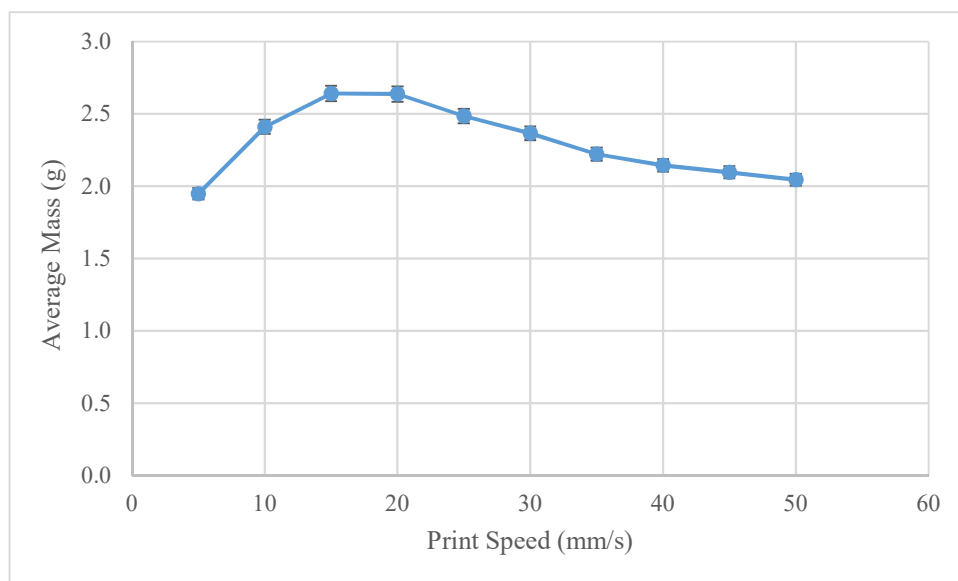


Figure 9. Virgin PLA–Average mass as a function of the print speed.

3.2.2. Reground 3-D Printed Parts PLA

The reground PLA was printed with the optimized settings that were found for virgin PLA. It printed well considering it had different types, colors, sizes, and shapes of particles being fed into it. The extruder did a good job of mixing the polymer inside the auger because the prints came out a consistent dark green color. Mechanical testing was conducted and it was found that the recycled PLA had a similar tensile strength to the virgin PLA, with the average being 38 MPA compared to 39 MPA for the virgin. This compares to studies by Cruz Sanchez et al. [31,32] where they showed that

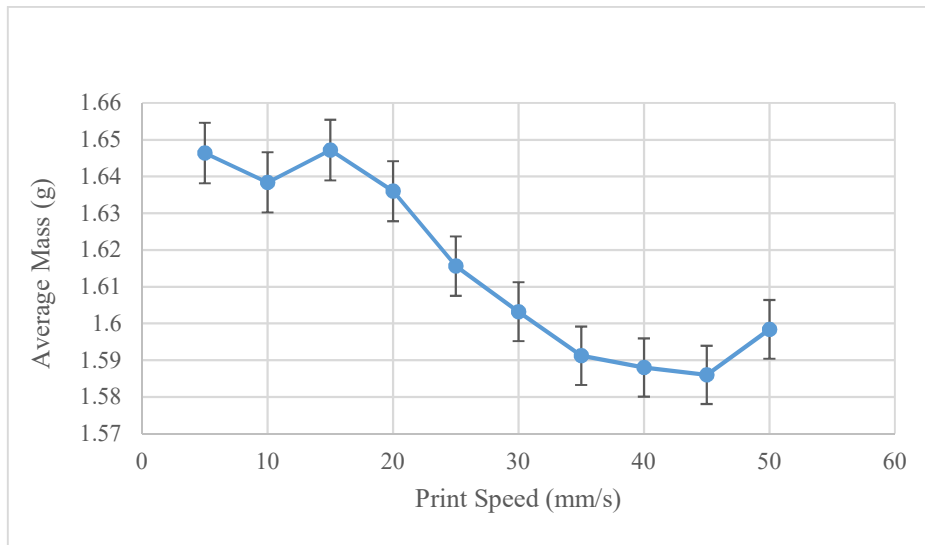


Figure 11. Recycled ABS-Average mass as a function of print speed.

3.2.4. Recycled PET Pellets

Material testing was conducted on ~4 mm recycled PET pellets. The results of this testing can be found in Figure 12. It should be noted that the ideal temperature settings of 220 °C and 230 °C were identified for zones 1 and 2. A bed temperature of 100 °C was found to achieve the best adhesion results.

Speed (mm/s)	Temperature (°C)																											
	Zone 2: 200 200 200 200 200 210 210 210 210 210														Zone 1: 200 210 220 230 240 240 230 220 210 200 200 200 210 220 230 240 240													
5	0.27	0.23	0.00	0.02	0.19	0.08	0.02	0.02	0.20	0.06	0.17	-0.14	-0.15	-0.14	0.04	-0.08	-0.16	0.11	0.49	-0.16	-0.22	-0.22	-0.27	-0.21	-0.08			
10	0.08	0.15	0.22	0.28	0.42	0.30	0.09	0.15	0.06	-0.21	0.29	-0.06	0.09	0.02	0.09	0.09	-0.08	0.14	0.24	-0.08	0.04	-0.18	-0.27	-0.09	-0.04			
15	0.06	0.31	0.27	0.13	0.12	0.20	-0.22	-0.08	0.02	0.22	0.06	0.13	0.02	0.12	0.15	0.21	0.00	0.12	0.13	-0.02	0.06	0.04	0.06	0.13	-0.12			
20	-0.02	-0.04	0.12	0.04	0.11	0.21	0.21	0.14	0.04	0.04	0.02	0.16	0.16	0.08	0.22	-0.18	0.21	0.14	-0.02	0.21	-0.08	0.06	-0.27	-0.04	0.00			
25	-2.42	-0.13	0.06	-0.02	0.18	0.17	-0.06	0.13	0.06	-0.19	-0.16	-0.06	0.06	0.02	-0.02	0.04	-0.02	0.11	-0.02	0.04	0.09	-0.12	0.00	0.11	-0.04			
30	-2.42	0.17	0.24	0.20	0.04	0.16	0.26	0.08	-0.12	-0.10	-0.06	0.04	0.12	0.22	0.21	0.28	0.21	0.00	0.04	-0.09	-0.02	0.11	0.02	0.31	0.24			
35	-2.42	-0.17	-2.42	0.00	0.04	-0.06	0.00	-0.21	-0.04	-0.23	-0.12	-0.06	0.02	-0.08	0.15	0.15	0.04	0.08	-0.04	-0.04	0.19	0.06	-0.26	0.13	-0.11			
40	-2.42	-2.42	-2.42	0.02	0.06	-0.06	-2.42	0.06	-0.12	-2.42	-0.24	0.09	-0.17	-0.06	0.04	0.17	-0.16	0.00	-0.12	-0.24	0.04	-0.18	-0.02	0.12	0.06			
45	-2.42	-2.42	-2.42	-0.04	0.04	0.21	-2.42	0.04	-0.15	-2.42	-0.23	-0.12	-0.11	0.15	-0.20	-0.04	-0.25	0.02	-0.06	-2.42	-0.08	-0.19	0.08	0.00	0.09			
50	-2.42	-2.42	-2.42	-2.42	0.04	0.22	-2.42	-0.04	-2.42	-2.42	-2.42	-0.04	-0.10	0.06	0.08	0.09	-0.15	0.11	0.06	-2.42	-0.09	-0.26	-0.10	0.12	0.02			
Average	-1.41	-0.67	-0.88	-0.18	0.12	0.14	-0.69	0.03	-0.25	-0.77	-0.27	-0.01	0.00	0.04	0.07	0.07	-0.04	0.08	0.07	-0.52	-0.01	-0.09	-0.10	0.06	0.00			
Abs. Value of Avg.	1.41	0.67	0.88	0.18	0.12	0.14	0.69	0.03	0.25	0.77	0.27	0.01	0.00	0.04	0.07	0.07	0.04	0.08	0.07	0.52	0.01	0.09	0.10	0.06	0.00			
Standard Deviation	1.23	1.15	1.26	0.75	0.11	0.11	1.13	0.10	0.73	1.09	0.73	0.10	0.11	0.10	0.11	0.13	0.14	0.05	0.17	0.95	0.11	0.13	0.14	0.13	0.10			

Best Temperature Settings

Figure 12. Recycled PET-difference between the theoretical and the actual mass of the line-speed temperature matrix.

Figure 13 shows that when printing with recycled PET, speeds between 5 mm/s and 30 mm/s have little difference in terms of average mass. When printing past 30 mm/s however, the mass substantially drops and, in some cases, when the temperatures were low, the extruder motor would skip and stall, causing the print to fail.

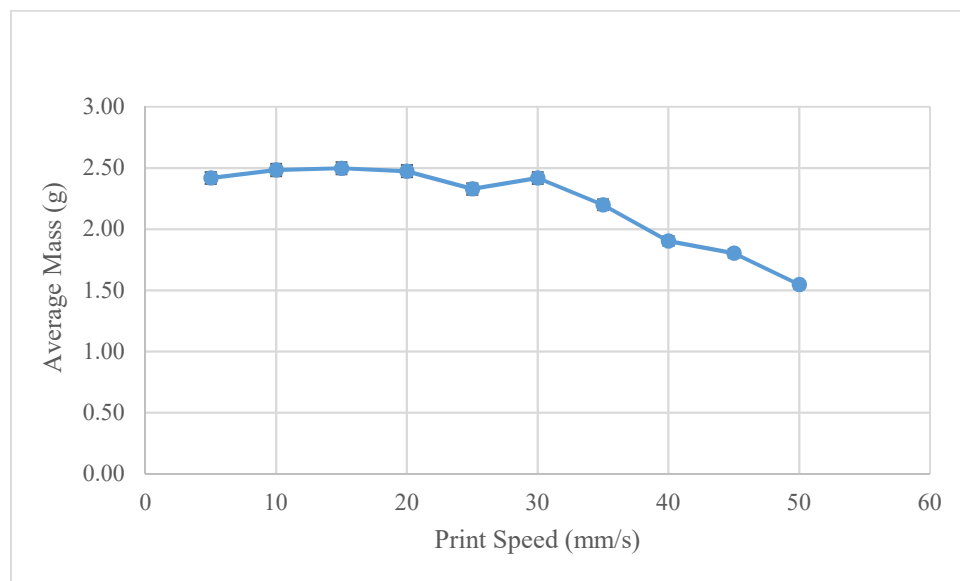


Figure 13. PET-Print speed effect on the printed line.

3.2.5. Recycled PP Chips

Reground PP chips were used to verify PP as a valid print material. The results of the matrix testing can be found in Figure 14, where the optimum print temperatures were found to be at 230 °C and 250 °C for heat zones 1 and 2, respectively.

Speed (mm/s)	Temperature (°C)																								
	Zone 2: 170 170 170 170 170 190 190 190 190 190										Zone 1: 170 190 210 230 250 170 190 210 230 250 170 190 210 230 250 170 190 210 230 250														
5	0.22	-0.21	-0.08	0.12	0.28	0.09	0.19	0.22	0.26	0.36	0.05	0.12	0.13	0.25	0.23	0.02	0.05	0.04	0.10	0.22	0.02	0.04	0.08	0.12	0.04
10	-0.15	-0.21	-0.18	-0.06	-0.02	0.12	0.18	0.20	0.26	0.29	0.11	0.13	0.15	0.25	0.23	0.09	0.11	0.12	0.17	0.20	0.12	0.06	0.09	0.14	0.15
15	-0.43	-0.45	-0.24	-0.08	0.11	0.11	0.17	0.22	0.24	0.27	0.11	0.17	0.16	0.26	0.24	0.06	0.18	0.17	0.16	0.22	0.16	0.16	0.13	0.14	0.15
20	-0.50	-0.66	-0.23	0.00	0.12	0.08	0.16	0.20	0.22	0.26	0.12	0.14	0.14	0.26	0.21	0.09	0.16	0.17	0.17	0.23	0.14	0.13	0.13	0.16	0.17
25	-0.63	-0.49	-0.14	-0.04	0.06	0.11	0.17	0.22	0.20	0.26	0.12	0.18	0.17	0.25	0.26	0.14	0.15	0.20	0.20	0.25	0.12	0.14	0.15	0.17	0.18
30	-1.66	-1.66	-0.05	-0.04	0.05	0.08	0.13	0.18	0.19	0.25	0.12	0.17	0.18	0.23	0.24	0.13	0.13	0.16	0.19	0.20	0.11	0.15	0.14	0.12	0.15
35	-1.66	-1.66	-0.03	-0.06	0.02	0.06	0.12	0.15	0.19	0.21	0.10	0.14	0.17	0.22	0.24	0.14	0.16	0.20	0.20	0.18	0.11	0.15	0.13	0.13	0.16
40	-1.66	-1.66	-0.08	0.03	-0.02	0.05	0.09	0.12	0.15	0.19	0.10	0.13	0.17	0.21	0.24	0.14	0.16	0.21	0.19	0.19	0.10	0.13	0.14	0.14	0.18
45	-1.66	-1.66	-0.02	-0.03	0.00	0.02	0.08	0.11	0.16	0.17	0.12	0.12	0.17	0.18	0.21	0.11	0.16	0.19	0.18	0.17	0.11	0.11	0.15	0.12	0.20
50	-1.66	-1.66	-1.66	0.07	0.09	0.02	0.05	0.13	0.13	0.17	0.11	0.12	0.19	0.18	0.21	0.03	0.11	0.18	0.18	0.20	0.11	0.09	0.16	0.15	0.20
Average	-0.98	-1.03	-0.27	-0.01	0.07	0.07	0.13	0.18	0.20	0.24	0.11	0.14	0.16	0.23	0.23	0.10	0.14	0.16	0.17	0.21	0.11	0.12	0.13	0.14	0.16
Abs. Value of Avg.	0.98	1.03	0.27	0.01	0.07	0.07	0.13	0.18	0.20	0.24	0.11	0.14	0.16	0.23	0.23	0.10	0.14	0.16	0.17	0.21	0.11	0.12	0.13	0.14	0.16
Standard Deviation	0.71	0.64	0.47	0.06	0.09	0.03	0.05	0.04	0.04	0.06	0.03	0.02	0.02	0.03	0.02	0.04	0.04	0.05	0.03	0.02	0.03	0.04	0.02	0.02	0.04

Best Temperature Settings

Figure 14. Reground PP-Difference between the theoretical and the actual mass of the line-speed temperature matrix.

When examining Figure 14, it should be pointed out that failures occurred when printing at too low of a temperature. The extruder motor stalled because of the high viscosity of the plastic at those temperatures. To prevent damage to the machine, the test was halted at the first sign of an extruder stall.

As seen in Figure 15, average line masses as a function of print speed, 30 mm/s was identified as the optimum print speed. Although, it should be pointed out that considering the overall magnitude of the mass scale, the weight is relatively insensitive to the print speed. At these settings, however, the volumetric printing speed is about 52.5 mm³/s, or has a deposition rate that is ~13 times faster than traditional FFF printing.

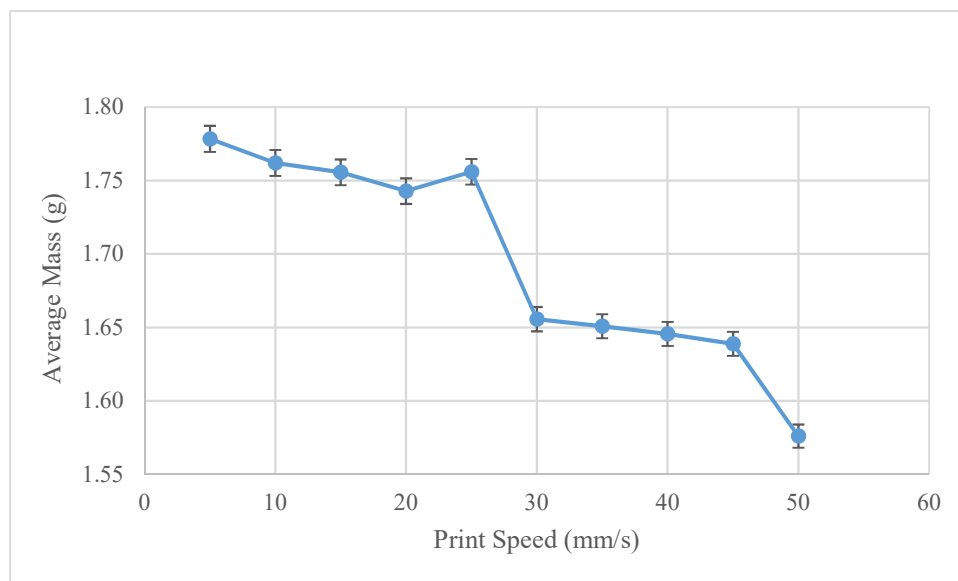


Figure 15. Recycled PP-Average mass as a function of print speed.

3.3. Mechanical Testing

The mechanical properties for PLA that is printed with FFF are comparable to what has been reported in standard FFF type printers where the tensile strength was found to be 47.55–50.23 MPa [66]. The average strain at the break (mm/mm) was 0.02 with a standard deviation of 0.01 for Type 1 and 0.02 with a standard deviation of 0.01 for Type 4. In addition, the modulus (MPa) was 2815 for Type 1 (SD 166.4) and 2135 (SD 273.5) for Type 4. Notably, peak stress for the Type 2 and Type 1 tensile bars was 43.35 (+/−5.89) and 39.43 (+/−5.22) MPa, which is close enough to consider the Type 4 tensile bars as being representative of the printed mechanical properties here. Recycled ABS had a peak stress of 26.40 MPa (SD 1.78), recycled PET had a peak stress of 40.63 MPa (SD 2.41), and recycled PP had a peak stress of 23.82 MPa (SD of 0.49).

PLA has a bulk tensile strength of 16 to 103 MPa [67], whereas 3-D printed PLA is 56.6 MPa [68], 50–57 MPa, depending on the color [69]. In this study, it was found that the virgin PLA Tensile Strength was on average 39 MPa, which is comparable to the average that was found with FFF/FDM style printers. The lower than average result can be explained by the large nozzle size of the Gigabot X and the fact that it cannot print small objects that are less than 20 mm by 20 mm without introducing gaps in complex geometries. The tensile bars had visible holes at the neck region where the printer would skip over because the geometry was too tight for the slicer to print it. This resulted in breaks happening outside of the extensometer, near the neck region of the bar, corrupting any elastic modulus data.

ABS has a bulk tensile strength of 20 to 73 MPa [70], whereas 3-D printed ABS ranged from around 25 to 32 MPa [71], 28.5 MPa [68]. In this study, the recycled ABS was found to have an average tensile strength of 26 MPa. This falls into the range of FFF/FDM style printers, meaning that printing from granules does not directly reduce the tensile strength.

PET has a bulk Tensile Strength of 47 to 90 MPa [72], whereas 3-D printed PET ranged from 27 to 45 MPa [73]. In this case, recycled PET was printed and the testing concluded that the average tensile strength was 40 MPa. Comparing this to FFF printed PET, it is actually on the high end, meaning that the recycled nature of the plastic did not have any significant impact on the strength of the material.

PP has a bulk tensile strength of 4 to 369 MPa [74], whereas 3-D printed PP ranged from 27 to 36 MPa [75]. PP was shown to have an average tensile strength of 24 MPa when it was printed with the Gigabot X. This is on the low end of both the bulk tensile strength and the FFF 3-D printed tensile strength, which could be explained by having more thermal cycles from numerous recycling processes and the purity of the PP, which are unknown with this specific plastic. This underscores the need for

better material ingredient tracking [76] and expanded recycling symbols [77] as the recycling of 3-D printed parts becomes more widespread.

4. Discussion

The advantages of printing with recycled particles rather than filament include lower costs, because of the lower cost of the starting material, and it is also easier to print large objects (e.g., where more than 1 spool of material is required) [78]. This has caused a recent surge in research that is related to 3-D printing with pellets including new printer designs: using a double stage screw [79], derivative of a metal injection molder [80,81], those based on RepRap technology [82], and industrial robots for 3-D printing [83], as well as a large range of polymers including conventional filament materials and recycled materials [82] as well as conductive polymer composites [84] and flexible materials [85]. These studies all indicate that FPF 3-D printing will play a larger role in the future of the 3-D printing industry and are corroborated by the results of this study.

The Gigabot X successfully printed with a wide range of particle sizes and distributions, which opens up a large array of starting materials beyond high-quality (e.g., uniform size and spherical) pellets. It can be concluded that the Gigabot X and similar FPF printers with good auger-barrel tolerances (± 0.025 mm) can handle a wide range of polymer inputs, including recycled materials with minimal post processing (i.e., only cleaning and grinding/shredding). In addition, due to the ease of extrusion and the ability to print in a wide distribution of particle sizes, this system is an ideal candidate for upcycling waste plastics and the development of unique plastics co-polymers and composites. The mechanical testing using tensile strength indicated that FPF did not degrade the polymer properties (e.g., similar to FFF), however, future work should also consider testing other mechanical properties such as compression, impact resistance, fracture toughness, creep testing, fatigue testing, and flexural strength. This will result in additional potential applications of recycled polymer FPF.

The ability to define multiple heating zones in the FPF extrusion system as in the Gigabot X is useful for multiple reasons. First, by establishing a pre-heating zone prior to extrusion, this helps to both transfer the required thermal energy to the plastic (given the high material flow rate) and to achieve sufficiently low viscosities for printing. The low viscosity also reduces motor wear from over torqueing and allows for faster material throughput during purging cycles. Another benefit of having multiple heating zones is to allow for more custom temperature profiles. Some plastics experience more shear heating than others. Therefore, having a descending temperature gradient would allow the temperature at the inlet to be higher to start melting and mixing the pellets as soon as possible to allow for the best throughput, while simultaneously setting the die heater at a lower temperature to prevent degradation from overheating in the shearing (metering) section. Changing the screw geometry or the compression ratio for every plastic would be very unsustainable, so being able to have control over how the different plastics flow while they are inside the extruder without having to replace the screw, comes down to controlling speed and temperature profiles.

The large format FPF type printer has unique abilities to print large components at high mass flow rates, resulting in dramatically shorter print times for large components. This is due to the ability to easily print with large nozzle sizes (1–2 mm). This is particularly useful in the manufacturing of large, functional components with non-critical surface smoothness criterion. Some applications include custom furniture, complete sporting goods equipment, large research tools, breathable casts and other health care products, agricultural processing equipment, OEM components, construction applications, and on demand fixtures or jigs.

There are, however, some limitations with this prototype system, including lower than normal FFF resolution in the x-y-plane (1.75 mm diameter minimum due to the nozzle diameter) and further limitations are imposed on the component size due to the high heat transfer rates from the large (comparative to traditional FFF printers) contact area of the printer's hot-end, meaning that parts that are less than 20 mm by 20 mm cannot be printed reliably. Useful future work would consider other

mechanisms for providing FPF beyond the system that has been described here. The Gigabot X is also currently lacking in any sort of part cooling system, which is a common feature on most FFF printers to assist in the cooling of the extruded plastics. This allows the printer to print complex geometries, such as overhangs of plastic, without losing dimensional accuracy or creating visual blemishes on the surface of the print. Without this, Gigabot X is limited in the geometries that it is capable of printing accurately. Finally, the prototype provides approximately six hours of continuous feed before manual replenishment. If this technology is to be scaled commercially, users would require much longer printing sessions and an automated feeding system.

Future work is needed to quantify the environmental benefits of using FPF over conventional FFF/FDM with both conventional filament as well as recycled filament. Several plastic pellet types and sizes from multiple vendors were used in this research. Significant variability in the size and the uniformity of the sourced pellets was observed between the different vendors. Further research on this hardware is needed to support supplier variability using non-uniform flake and/or pellets. Finally, a detailed cost analysis is needed to quantify the economic benefits of utilizing this approach.

5. Conclusions

The Gigabot X system presents a uniquely robust open source solution to large format FPF printing. Notable with this design was the ability to print a large variety of polymers at dramatically lower print times when compared to traditional FFF type printing. As recycled plastic and pellets are less costly than filament, this system succeeds in lowering the economic barriers to the fabrication of large format, high value, plastic components, which has been an unfulfilled gap in the open source, distributed manufacturing design space.

The tensile strengths of the printed parts for traditional FFF/FDM prints and the FPF prints are comparable for all of the polymers that were tested when the melt/print cycles are taken into account. This means that there will be no need to sacrifice part strength by using FPF systems. More studies need to be conducted to determine how the layer adhesion compares between an FFF and an FPF system.

Finally, a novel methodology was tested to successfully operate any FPF system (and the Gigabot X in particular) to experimentally determine the best 3-D printing parameters for new polymers. The line test was developed to show the best temperatures to print the new polymer regardless of type or particle size distribution. The single walled vase test was used to determine the theoretical vs actual mass and to get a flow percentage that would calibrate the extruder. The vase test was also used to determine the actual extrusion width to be put into Slic3r to prevent overlapping lines or under-extrusion. These simple tests can be performed over the course of a couple days for any unknown polymer and, once completed, should give the correct settings for successful prints.

Author Contributions: Conceptualization, J.M.P.; Data curation, A.L.W. and D.J.B.; Formal analysis, A.L.W., D.J.B., R.B.O., M.J.F., S.L.S. and J.M.P.; Funding acquisition, S.L.S. and J.M.P.; Methodology, A.L.W., D.J.B. and J.M.P.; Project administration, S.L.S.; Writing-original draft, A.L.W., D.J.B. and J.M.P.; Writing-review & editing, A.L.W., D.J.B., R.B.O., M.J.F., S.L.S. and J.M.P.

Funding: This research was funded by NSF SBIR Phase I grant number: 1746480 and the WeWork Global Creator Award.

Conflicts of Interest: Robert B. Oakley, Matthew J. Fiedler and Samantha L. Snabes are employees of re:3D, which manufactures the Gigabot X that was used in this study. All of the data was collected by the authors from MTU, who have no conflict of interest. The funders played no part in the design of the study, in the collection, analyses, or interpretation of the data, in the writing of the manuscript, or in the decision to publish the results.

References

1. Sells, E.; Bailard, S.; Smith, Z.; Bowyer, A.; Olliver, V. RepRap: The Replicating Rapid Prototyper-Maximizing Customizability by Breeding the Means of Production. In Proceedings of the World Conference on Mass Customization and Personalization, Cambridge, MA, USA, 7–10 October 2007.

2. Jones, R.; Haufe, P.; Sells, E.; Irvani, P.; Olliver, V.; Palmer, C.; Bowyer, A. RepRap—the Replicating Rapid Prototyper. *Robotica* **2011**, *29*, 177–191. [[CrossRef](#)]
3. Bowyer, A. 3D Printing and Humanity’s First Imperfect Replicator. *3D Print. Addit. Manuf.* **2014**, *1*, 4–5. [[CrossRef](#)]
4. Scan, B. How to Make (almost) Anything. *The Economist*. 2005. Available online: https://www.economist.com/node/4031304/print?Story_ID=40313044031304 (accessed on 9 August 2018).
5. Gershenfeld, N. How to Make Almost Anything: The Digital Fabrication Revolution. 2012. Available online: <http://cba.mit.edu/docs/papers/12.09.FA.pdf> (accessed on 9 August 2018).
6. Markillie, P. A Third Industrial Revolution. *The Economist*. 2012. Available online: <https://www.economist.com/special-report/2012/04/21/a-third-industrial-revolution> (accessed on 9 August 2018).
7. Gwamuri, J.; Wittbrodt, B.; Anzalone, N.; Pearce, J. Reversing the Trend of Large Scale and Centralization in Manufacturing: The Case of Distributed Manufacturing of Customizable 3-D-Printable Self-Adjustable Glasses. *Chall. Sustain.* **2014**, *2*, 30–40. [[CrossRef](#)]
8. Wittbrodt, B.; Laureto, J.; Tymrak, B.; Pearce, J. Distributed Manufacturing with 3-D Printing: A Case Study of Recreational Vehicle Solar Photovoltaic Mounting Systems. *J. Frugal Innov.* **2015**, *1*, 1–7. [[CrossRef](#)]
9. Woern, A.L.; Pearce, J.M. Distributed Manufacturing of Flexible Products: Technical Feasibility and Economic Viability. *Technologies* **2017**, *5*, 71. [[CrossRef](#)]
10. Petersen, E.E.; Kidd, R.W.; Pearce, J.M. Impact of DIY Home Manufacturing with 3D Printing on the Toy and Game Market. *Technologies* **2017**, *5*, 45. [[CrossRef](#)]
11. Petersen, E.E.; Pearce, J. Emergence of Home Manufacturing in the Developed World: Return on Investment for Open-Source 3-D Printers. *Technologies* **2017**, *5*, 7. [[CrossRef](#)]
12. Wittbrodt, B.T.; Glover, A.G.; Laureto, J.; Anzalone, G.C.; Oppliger, D.; Irwin, J.L.; Pearce, J.M. Life-cycle economic analysis of distributed manufacturing with open-source 3-D printers. *Mechatronics* **2013**, *23*, 713–726. [[CrossRef](#)]
13. Anderson, P.; Sherman, C.A. A discussion of new business models for 3D printing. *Int. J. Technol. Mark.* **2007**, *2*, 280–294. [[CrossRef](#)]
14. Laplume, A.; Anzalone, G.; Pearce, J. Open-source, self-replicating 3-D printer factory for small-business manufacturing. *Int. J. Adv. Manuf. Technol.* **2015**, *85*, 633–642. [[CrossRef](#)]
15. Laplume, A.; Petersen, B.; Pearce, J. Global value chains from a 3D printing perspective. *J. Int. Bus. Stud.* **2016**, *47*, 595–609. [[CrossRef](#)]
16. Pearce, J. Building Research Equipment with Free, Open-Source Hardware. *Science* **2012**, *337*, 1303–1304. [[CrossRef](#)] [[PubMed](#)]
17. Pearce, J. *Open-Source Lab.: How to Build Your Own Hardware and Reduce Research Costs*, 1st ed.; Elsevier: Waltham, MA, USA, 2014.
18. Baden, T.; Chagas, A.; Marzullo, T.; Prieto-Godino, L.; Euler, T. Open Laware: 3-D Printing Your Own Lab Equipment. *PLoS Biol.* **2015**, *13*, e1002175.
19. Dhankani, K.C.; Pearce, J.M. Open source laboratory sample rotator mixer and shaker. *Hardware X* **2017**, *1*, 1–12. [[CrossRef](#)]
20. Coakley, M.; Hurt, D.E. 3D Printing in the Laboratory: Maximize Time and Funds with Customized and Open-Source Labware. *J. Lab. Autom.* **2016**, *21*, 489–495. [[CrossRef](#)] [[PubMed](#)]
21. Pearce, J. Quantifying the Value of Open Source Hardware Development. *Mod. Econ.* **2015**, *6*, 1–11. [[CrossRef](#)]
22. Pearce, J.M. Return on investment for open source scientific hardware development. *Sci. Pub. Policy* **2016**, *43*, 192–195. [[CrossRef](#)]
23. *Wohlers Report 2016: 3D Printing and Additive Manufacturing State of the Industry Annual Worldwide Progress Report*; Wohlers Associates Inc.: Fort Collins, CO, USA, 2016.
24. Baechler, C.; DeVuono, M.; Pearce, J.M. Distributed recycling of waste polymer into RepRap feedstock. *Rapid Prototyp. J.* **2013**, *19*, 118–125. [[CrossRef](#)]
25. Kreiger, M.; Anzalone, G.C.; Mulder, M.L.; Glover, A.; Pearce, J.M. Distributed recycling of post-consumer plastic waste in rural areas. *MRS Online Proc.* **2013**, *1492*, 91–96. [[CrossRef](#)]
26. Kreiger, M.A.; Mulder, M.L.; Glover, A.G.; Pearce, J.M. Life cycle analysis of distributed recycling of post-consumer high density polyethylene for 3-D printing filament. *J. Clean. Prod.* **2014**, *70*, 90–96. [[CrossRef](#)]

27. Zhong, S.; Rakhe, P.; Pearce, J.M. Energy Payback Time of a Solar Photovoltaic Powered Waste Plastic Recyclebot System. *Recycling* **2017**, *2*, 10. [[CrossRef](#)]
28. Zhong, S.; Pearce, J.M. Tightening the loop on the circular economy: Coupled distributed recycling and manufacturing with recyclebot and RepRap 3-D printing. *Resour. Conserv. Recycl.* **2018**, *128*, 48–58. [[CrossRef](#)]
29. Recyclebot. Appropedia. Available online: <http://www.appropedia.org/Recyclebot> (accessed on 9 August 2018).
30. Woern, A.L.; McCaslin, J.R.; Pringle, A.M.; Pearce, J.M. RepRapable Recyclebot: Open source 3-D printable extruder for converting plastic to 3-D printing filament. *Hardware X* **2018**, *4*, e00026. [[CrossRef](#)]
31. Cruz Sanchez, F.; Lanza, S.; Boudaoud, H.; Hoppe, S.; Camargo, M. Polymer Recycling and Additive Manufacturing in an Open Source context: Optimization of processes and methods. In Proceedings of the 2015 Annual International Solid Freeform Fabrication Symposium—An Additive Manufacturing Conference, Austin, TX, USA, 10–12 August 2015; pp. 10–12.
32. Cruz Sanchez, F.A.; Boudaoud, H.; Hoppe, S.; Camargo, M. Polymer recycling in an open-source additive manufacturing context: Mechanical issues. *Add. Manuf.* **2017**, *17*, 87–105. [[CrossRef](#)]
33. Anderson, I. Mechanical Properties of Specimens 3D Printed with Virgin and Recycled Polylactic Acid. *3D Print. Add. Manuf.* **2017**, *4*, 110–115. [[CrossRef](#)]
34. Pakkanen, J.; Manfredi, D.; Minetola, P.; Iuliano, L. About the Use of Recycled or Biodegradable Filaments for Sustainability of 3D Printing. In *Sustainable Design and Manufacturing, Smart Innovation, Systems and Technologies*; Springer: Cham, Switzerland, 2017; pp. 776–785.
35. Chong, S.; Pan, G.-T.; Khalid, M.; Yang, T.C.-K.; Hung, S.-T.; Huang, C.-M. Physical Characterization and Pre-assessment of Recycled High-Density Polyethylene as 3D Printing Material. *J. Polym. Environ.* **2017**, *25*, 136–145. [[CrossRef](#)]
36. Mohammed, M.I.; Mohan, M.; Das, A.; Johnson, M.D.; Badwal, P.S.; McLean, D.; Gibson, I. A low carbon footprint approach to the reconstitution of plastics into 3D-printer filament for enhanced waste reduction. *KnE Eng.* **2017**, *2*, 234–241. [[CrossRef](#)]
37. Mohammed, M.I.; Das, A.; Gomez-Kervin, E.; Wilson, D.; Gibson, I. EcoPrinting: Investigating the use of 100% recycled Acrylonitrile Butadiene Styrene (ABS) for Additive Manufacturing. Solid Freeform Fabrication 2017. In Proceedings of the 28th Annual International Solid Freeform Fabrication Symposium, Austin, TX, USA, 7–9 August 2017.
38. Pringle, A.M.; Rudnicki, M.; Pearce, J. Wood Furniture Waste-Based Recycled 3-D Printing Filament. *For. Prod. J.* [[CrossRef](#)]
39. Tian, X.; Liu, T.; Wang, Q.; Dilmurat, A.; Li, D.; Ziegmann, G. Recycling and remanufacturing of 3D printed continuous carbon fiber reinforced PLA composites. *J. Clean. Prod.* **2017**, *142*, 1609–1618. [[CrossRef](#)]
40. Oblak, P.; Gonzalez-Gutierrez, J.; Zupančič, B.; Aulova, A.; Emri, I. Processability and mechanical properties of extensively recycled high density polyethylene. *Polym. Degrad. Stab.* **2015**, *114*, 133–145. [[CrossRef](#)]
41. Hyung Lee, J.; Sub Lim, K.; Gyu Hahm, W.; Hun Kim, S. Properties of recycled and virgin poly(ethylene terephthalate) blend fibers. *Appl. Polym. Sci.* **2012**, *128*, 2.
42. Beaudoin, A. JMS-1704: Multihead 3D Printer. Ph.D. Thesis, Worcester Polytechnic Institute Worcester, Worcester, MA, USA, 2016.
43. Volpato, N.; Kretschek, D.; Foggiatto, J.A.; da Silva Cruz, C.G. Experimental analysis of an extrusion system for additive manufacturing based on polymer pellets. *Int. J. Adv. Manuf. Technol.* **2015**, *81*, 1519–1531. [[CrossRef](#)]
44. Whyman, S.; Arif, K.M.; Potgieter, J. Design and development of an extrusion system for 3D printing biopolymer pellets. *Int. J. Adv. Manuf. Technol.* **2018**, *96*, 3417–3428. [[CrossRef](#)]
45. Horne, R. Reprap Development and Further Adventures in DIY 3D Printing: No More Filament? -Quest for a Universal Pellet Extruder for 3D Printing. Reprap development and further adventures in DIY 3D printing 2014. Available online: <https://richrap.blogspot.com/2014/12/no-more-filament-quest-for-universal.html> (accessed on 9 August 2018).
46. Universal Pellet Extruder. Available online: <http://upe3d.blogspot.com/> (accessed on 9 August 2018).
47. The PartDaddy-Large Format Delta 3D Printer-Custom. Available online: <https://www.seemecnc.com/products/partdaddy-large-format-delta-3d-printer> (accessed on 9 August 2018).
48. Cheetah Pro Large Format 3D Printer by Hans Fouche. Available online: <http://www.fouche3dprinting.com> (accessed on 9 August 2018).

49. Introducing David. Available online: <http://sculptify.com/david> (accessed on 9 July 2018).
50. Erecto-Struder 24v, ErectorBot Store. Available online: http://www.erecortorbot.com/store/product_info.php?cPath=23&products_id=65 (accessed on 9 August 2018).
51. Gigabot X: Large-Scale, Recycled Plastic Pellet 3D Printer. Available online: <https://www.kickstarter.com/projects/re3d/gigabot-x-your-direct-pellet-extrusion-3d-printer> (accessed on 9 August 2018).
52. Hopewell, J.; Dvorak, R.; Kosior, E. Plastics recycling: challenges and opportunities. *Philos. Trans. R. Soc. Lond. B Biol. Sci.* **2009**, *364*, 2115–2126. [CrossRef] [PubMed]
53. OSHE Granulator MKII, Open Science Framework. Available online: <https://osf.io/auswp/> (accessed on 9 August 2018).
54. Fiji is just ImageJ. Available online: <https://fiji.sc/> (accessed on 9 August 2018).
55. Re:3D. Available online: <https://github.com/Gigabot-Labs/Pellet-Extruder> (accessed on 9 August 2018).
56. Re:3D. Life-Sized Affordable 3D Printing. Available online: <https://re3d.org/> (accessed on 9 August 2018).
57. Slic3r-G-Code Generator for 3D Printers. Available online: <http://slic3r.org> (accessed on 9 August 2018).
58. Marlin Firmware. Available online: <http://marlinfw.org> (accessed on 9 August 2018).
59. RepRap PLA. Available online: <https://reprap.org/wiki/PLA> (accessed on 9 August 2018).
60. RepRap ABS. Available online: <https://reprap.org/wiki/ABS> (accessed on 9 August 2018).
61. Matter Hackers. 3D Printer Filament Comparison Guide. Available online: <https://www.matterhackers.com/3d-printer-filament-compare> (accessed on 9 August 2018).
62. Available online: <https://osf.io/fsjk9/> (accessed on 9 August 2018).
63. LeapFrog. 3D Printing with Polypropylene. Available online: <https://www.lpfrg.com/en/3d-printing-polypropylene> (accessed on 9 August 2018).
64. Laureto, J.J.; Pearce, J.M. Anisotropic mechanical property variance between ASTM D638-14 type i and type iv fused filament fabricated specimens. *Polym. Test.* **2018**, *68*, 294–301. [CrossRef]
65. Giles, H.; Wagner, J.; Eldridge, M. *Extrusion-The Definitive Processing Guide and Handbook*; Elsevier: Amsterdam, The Netherlands, 2005; p. 67.
66. Raj, S.; Muthukumar, E.; Jayakrishna, K. A Case Study of 3D Printed PLA and Its Mechanical Properties. *Proceedings* **2018**, *5*, 11219–11226. [CrossRef]
67. MatWeb-Overview of Materials for Polylactic Acid (PLA) Biopolymer. Available online: <http://www.matweb.com/search/DataSheet.aspx?MatGUID=ab96a4c0655c4018a8785ac4031b9278&ckck=1> (accessed on 9 August 2018).
68. Tymrak, B.M.; Kreiger, M.; Pearce, J.M. Mechanical properties of components fabricated with open-source 3-D printers under realistic environmental conditions. *Mater. Des.* **2014**, *58*, 242–246. [CrossRef]
69. Wittbrodt, B.; Pearce, J.M. The effects of PLA color on material properties of 3-D printed components. *Add. Manuf.* **2015**, *8*, 110–116. [CrossRef]
70. MatWeb-Overview of Materials for Acrylonitrile Butadiene Styrene (ABS), Molded. Available online: <http://www.matweb.com/search/DataSheet.aspx?MatGUID=eb7a78f5948d481c9493a67f0d089646> (accessed on 9 August 2018).
71. Tanikella, N.G.; Wittbrodt, B.; Pearce, J.M. Tensile strength of commercial polymer materials for fused filament fabrication 3D printing. *Add. Manuf.* **2017**, *15*, 40–47. [CrossRef]
72. MatWeb-Overview of Materials for Polyethylene Terephthalate (PET), Unreinforced. Available online: <http://www.matweb.com/search/DataSheet.aspx?MatGUID=a696bdcdff6f41dd98f8eec3599eaa20> (accessed on 9 August 2018).
73. Zander, N.; Gillan, M.; Lambeth, R. Recycled polyethylene terephthalate as a new FFF feedstock material. *Add. Manuf.* **2018**, *21*, 174–182. [CrossRef]
74. MatWeb-Overview of Materials for Polypropylene, Molded. Available online: <http://www.matweb.com/search/DataSheet.aspx?MatGUID=08fb0f47ef7e454fbf7092517b2264b2> (accessed on 9 August 2018).
75. Carneiro, O.; Silva, A.; Gomes, R. Fused deposition modeling with polypropylene. *Mater. Des.* **2015**, *2015*, 83, 768–776. [CrossRef]
76. Pearce, J.M. Expanding the Consumer Bill of Rights for material ingredients. *Mater. Today* **2018**, *21*, 197–198. [CrossRef]
77. Hunt, E.J.; Zhang, C.; Anzalone, N.; Pearce, J.M. Polymer recycling codes for distributed manufacturing with 3-D printers. *Resour. Conserv. Recycl.* **2015**, *97*, 24–30. [CrossRef]

78. Stevenson, K. The Other Reason for 3D Printing Pellets. Fabbaloo. Available online: <http://www.fabbaloo.com/blog/2018/5/10/the-other-reason-for-3d-printing-pellets> (accessed on 9 August 2018).
79. Liu, X.; Chi, B.; Jiao, Z.; Tan, J.; Liu, F.; Yang, W. A large-scale double-stage-screw 3D printer for fused deposition of plastic pellets. *J. Appl. Polym. Sci.* **2017**, *134*, 45147. [[CrossRef](#)]
80. Giberti, H.; Sbaglia, L.; Silvestri, M. Mechatronic Design for an Extrusion-Based Additive Manufacturing Machine. *Machines* **2017**, *5*, 29. [[CrossRef](#)]
81. Giberti, H.; Sbaglia, L. A Robotic Design for a MIM Based Technology. In *Advances in Service and Industrial Robotics; Mechanisms and Machine Science*; Springer: Cham, Switzerland, 2017; pp. 565–572.
82. Braanker, G.B.; Duwel, J.E.P.; Flohil, J.J.; Tokaya, G.E. Developing a plastics recycling add-on for the RepRap 3D-printer. Delft University of Technology, 2010. Available online: <https://reprapdelft.files.wordpress.com/2010/04/reprap-granule-extruder-tudelft1.pdf> (accessed on 9 August 2018).
83. Wang, Z.; Liu, R.; Sparks, T.; Liou, F. Large-Scale Deposition System by an Industrial Robot (I): Design of Fused Pellet Modeling System and Extrusion Process Analysis. *3D Print. Add. Manuf.* **2016**, *3*, 39–47. [[CrossRef](#)]
84. Kumar, N.; Jain, P.K.; Tandon, P.; Pandey, P.M. Additive manufacturing of flexible electrically conductive polymer composites via CNC-assisted fused layer modeling process. *J. Braz. Soc. Mech. Sci. Eng.* **2018**, *40*, 175. [[CrossRef](#)]
85. Kumar, N.; Jain, P.K.; Tandon, P.; Pandey, P.M. Extrusion-based additive manufacturing process for producing flexible parts. *J. Braz. Soc. Mech. Sci. Eng.* **2018**, *40*, 143. [[CrossRef](#)]



© 2018 by the authors. Licensee MDPI, Basel, Switzerland. This article is an open access article distributed under the terms and conditions of the Creative Commons Attribution (CC BY) license (<http://creativecommons.org/licenses/by/4.0/>).